Electronic Supplementary Information (ESI) for Lab on a Chip

Electronic Supplementary Information

An integrated microfluidic system for studying cell-microenvironmental interactions versatilely and dynamically

Wenming Liu,[a] Li Li,[a] Xuming Wang,[b] Li Ren,[a] Xueqin Wang,[a] Jianchun Wang,[c] Qin Tu,[c] Xiaowen Huang[a] and Jinyi Wang*[acd]

[a]*College of Animal Medicine, Northwest A&F University, Yangling, Shaanxi, 712100, China*

[b]*College of Life Science, Northwest A&F University, Yangling, Shaanxi, 712100, China*

[c]*College of Science, Northwest A&F University, Yangling, Shaanxi, 712100, China*

[d]*Shaanxi Key Laboratory of Molecular Biology for Agriculture, Yangling, Shaanxi, 712100, China*

Abstract. This supplementary information includes all of the additional information as noted in the paper and more detailed discussion on the current study.

ESI Movies

Movie S1. Individual addressability of the chambers in the microfluidic system. Video microscopic imaging of food dyes of four different colors (red, yellow, green, and blue) being alternatively fed to consecutive chambers using the microfluidic multiplexer and pressure-driven flow (accelerated to six times the actual speed). This demonstrates how different surface treatment reagents, media, conditional solution, staining reagents, or cells can be delivered to different chambers without cross-contamination.

Movie S2. Controllable communication of chambers in the microfluidic system. Video microscopic imaging showing the real-time control of chamber communication visualized through different dyed solutions (red, yellow, green, and blue) through the connective channels using groups of microvalves (accelerated to 2 times the actual speed). This demonstrates that directional communication of cell-related reasearch, especially cell-environmental interactions, can be performed here in real-time.

Movie S3. Real-time conditional transition. Video microscopic imaging showing the process of addressable replacement visualized through different dyed solutions (red, yellow, green, and blue) using the microfluidic multiplexer and pressure-driven flow (accelerated to 2 times the actual speed). This demonstrates how multi-step research on cell-environmental interactions can be carried out in a sequential and temporal manner.

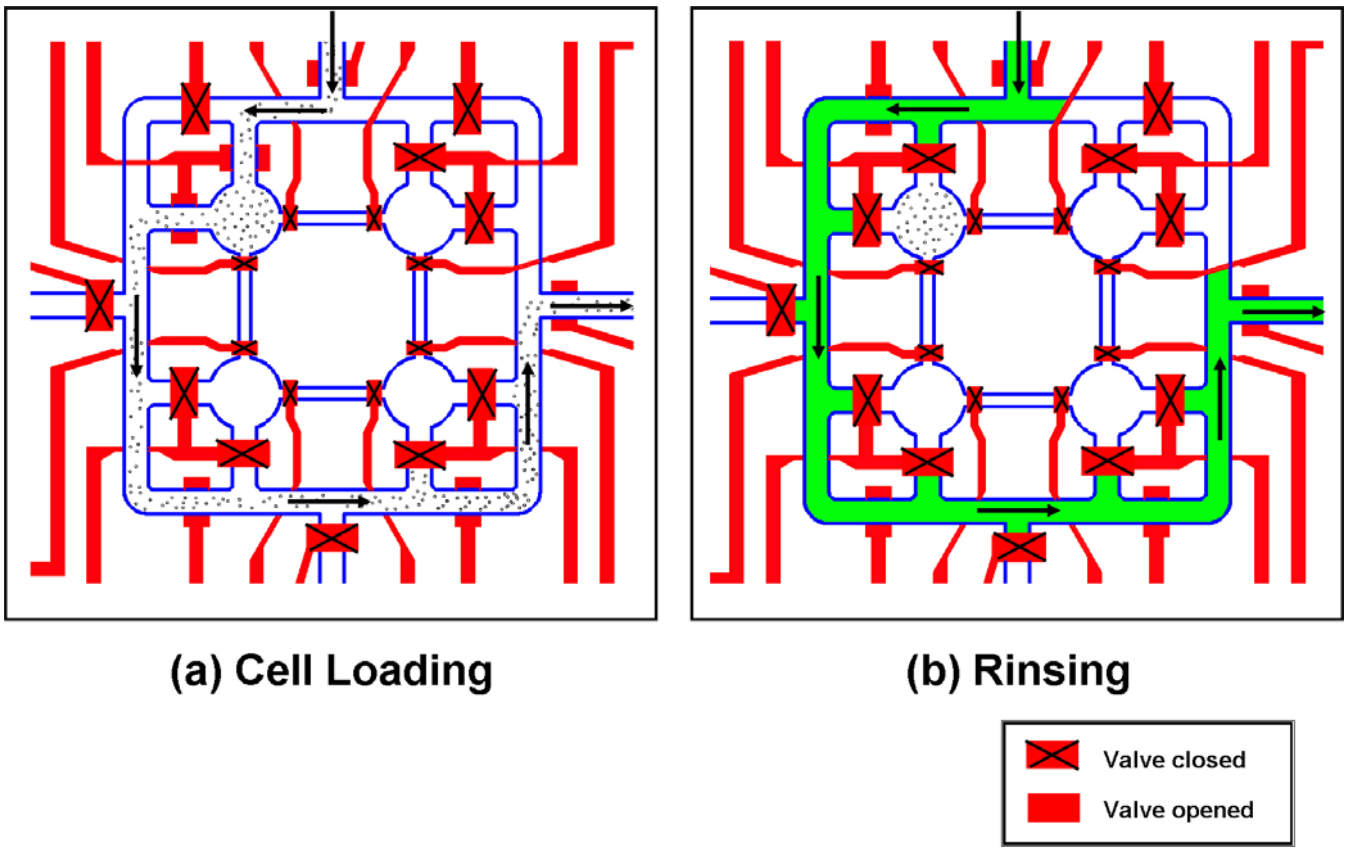

Fig. S1. Schematic diagrams illustrating the cell introduction and rinsing procedure. We used a one-way path model to perform flow delivery that coordinated the opening and closing of the microvalves appropriately. (a) All cells passed through the chamber with no escaping to the non-targeted chambers; some adhered on the surface of the collagen-modified chamber. (b) The residue of those in the channels was removed by a rinsing process.

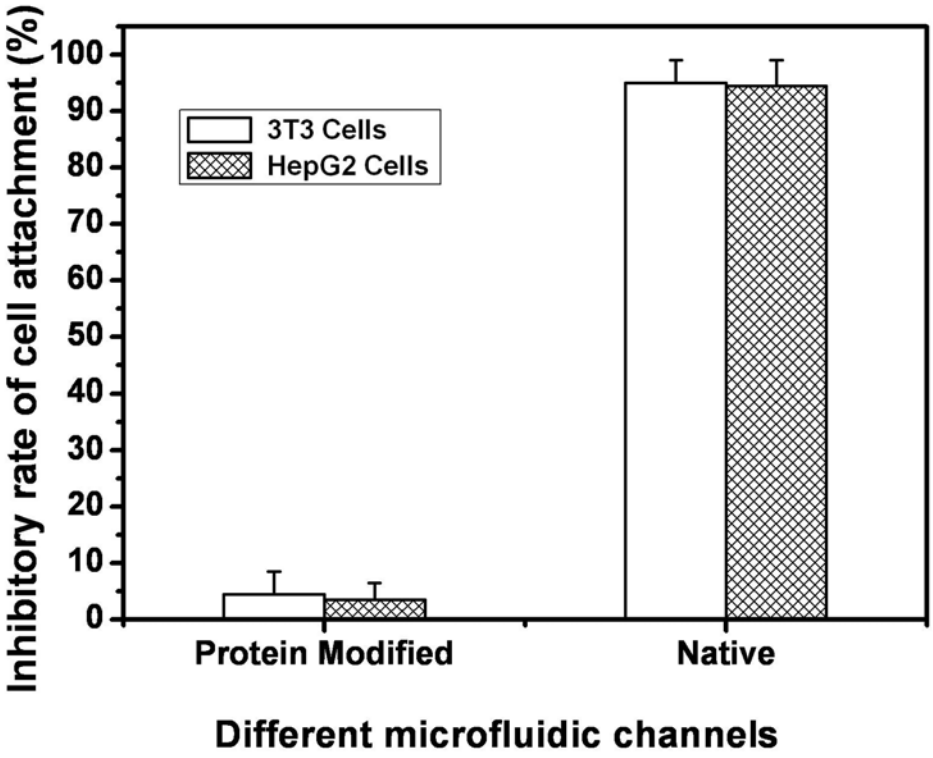

Fig. S2. Inhibitory rate of cell attachment in both collagen-modified and native PDMS microchannel surfaces at the flow velocity of delivery (2 μl/min). In this study, collagen-I, a popular extracellular matrix protein, was utilized to modify the cell-culture chambers specifically and locally to improve cell attachment and cultivation without large retention of cells in non-modified transporting channels (Gómez-Sjöberg, et al. *Anal. Chem.*, 2007, **79**, 8557-8563). Results show that it can greatly reduce the stay of cells in the non-targeted channel. We defined zero cell attachment as 100% of the inhibitory rate.

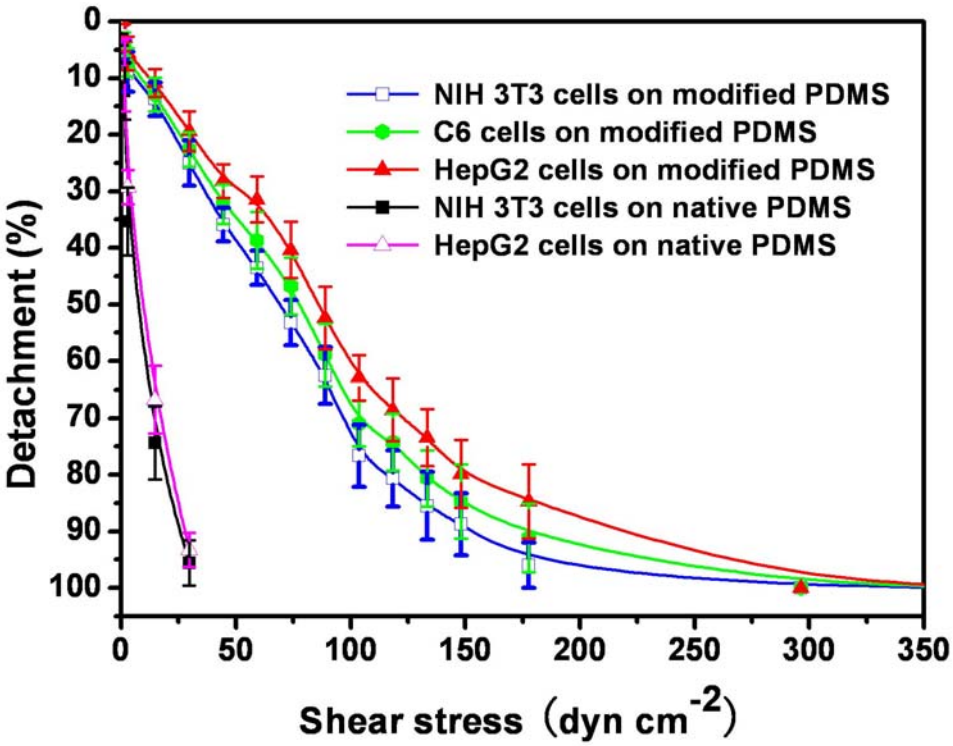

Fig. S3. Detachment of three types of cells (NIH 3T3 fibroblasts, HepG2 carcinoma cells, and C6 glioma cells) from non-modified (native) and collagen-modified PDMS microchannel surfaces as a function of shear stress after incubation for 30 min at 37□. Shear stress and its relationship with cell detachment were determined following the methods reported previously (Zhang, et al. *Chem. Eng. J.*, 2008, **135S**, S82-S88; Schneider, et al. *Biomed. Microdevices*, 2001, **3**, 315-322; Riddle, et al. *Am. J. Physiol. Cell Physiol.* 2006, **290**, C776-784). Shear stress was directly proportional to the flow velocity. High-velocity corresponds to high shear stress. Results show that cells in non-modified PDMS microchannel could be easily removed by increasing the flow velocity. In the current study, the flow velocity used for rinsing after cells loading was 15 μl/min. Its corresponding shear stress was 34.2 dyn/cm^2.

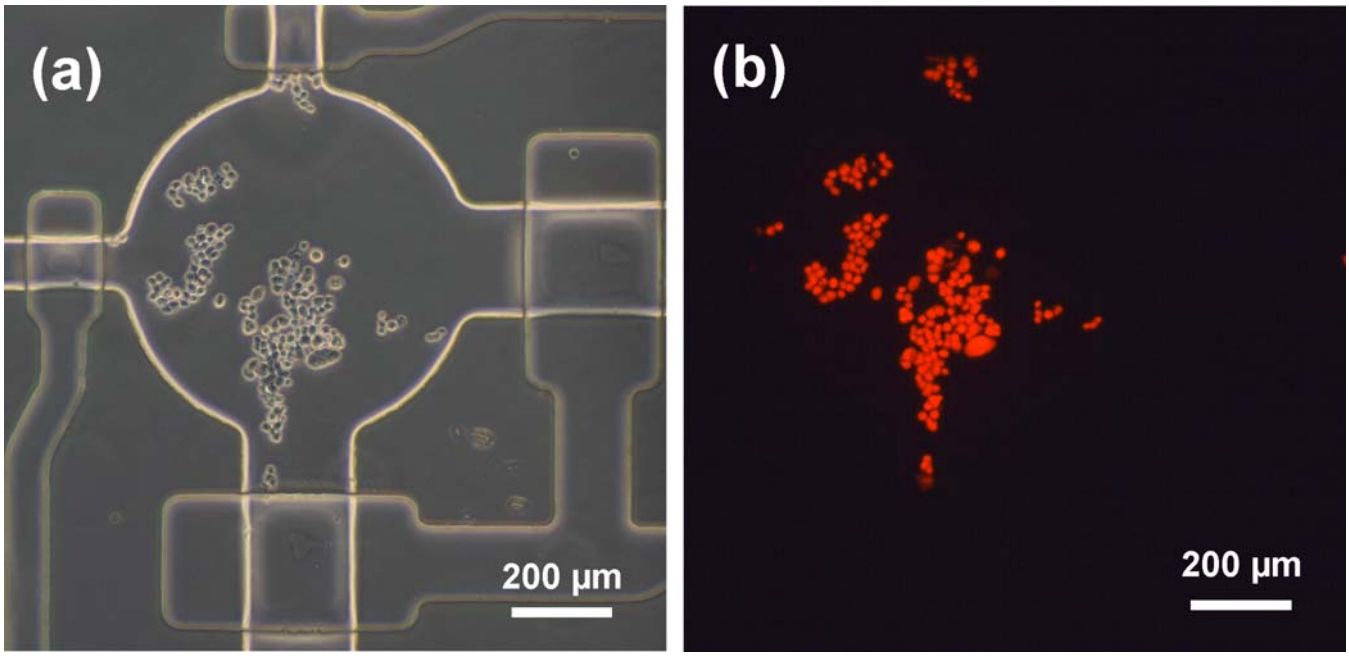

Fig. S4. Optical image (a) and PI-stained fluorescence image (b) of NIH 3T3 cells just localized in a microchamber. The microvalves can be used as the functional obstacle for cell trapping.

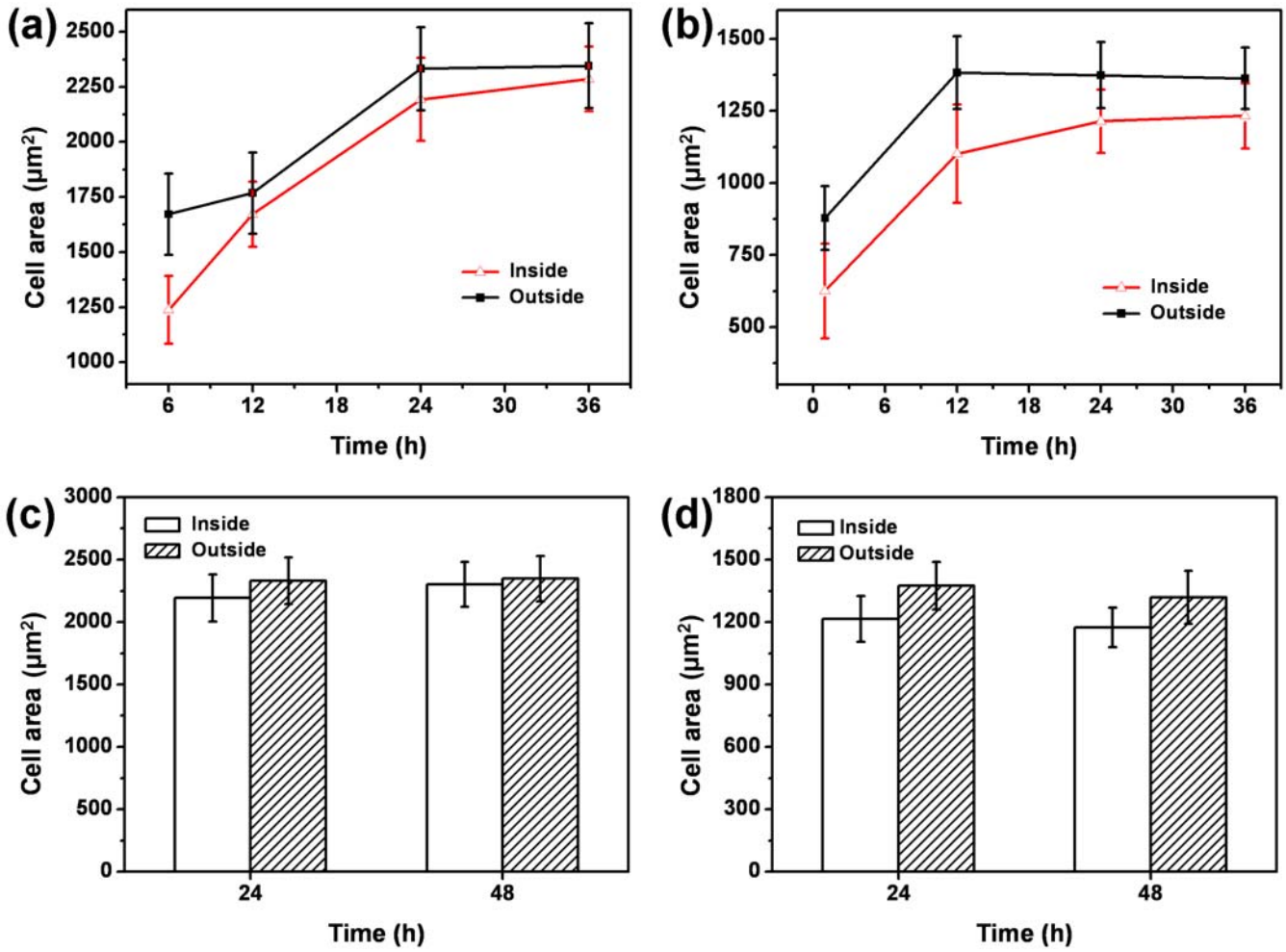

Fig. S5. Comparative spreading area of cells cultivated in a microchamber (inside) and a normal 24-well plate (outside). (a) and (c) NIH 3T3 fibroblasts; (b) and (d) HepG2 carcinoma cells.

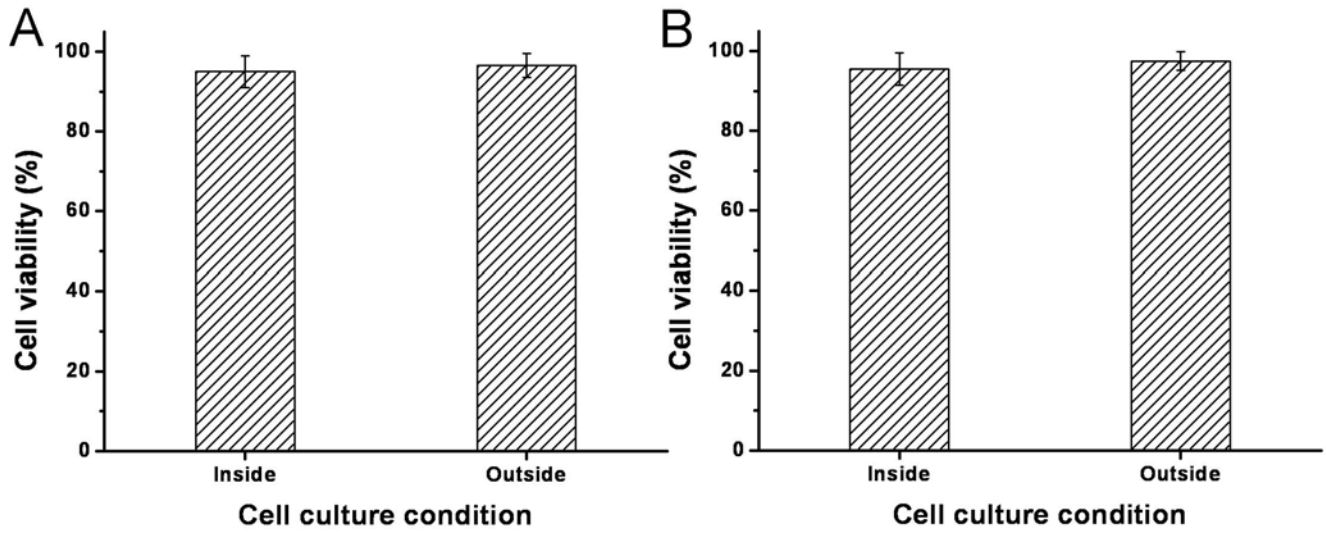

Fig. S6. (A) Cell viability of HepG2 carcinoma cells cultivated in a microchamber (inside) and a normal 24-well plate (outside). (B) Cell viability of NIH 3T3 fibroblasts cultivated in a microchamber (inside) and a normal 24-well plate (outside).

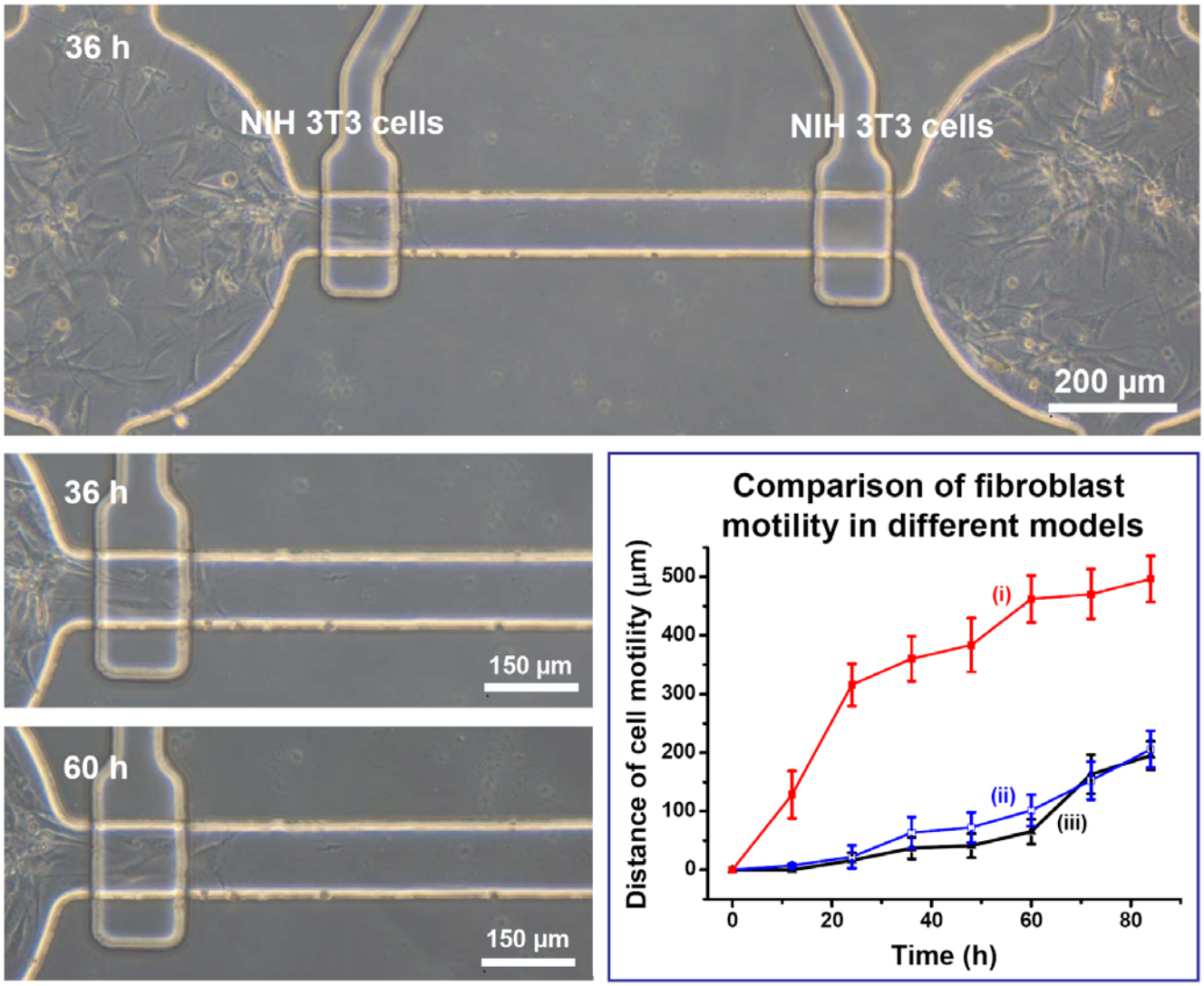

Fig. S7. Assay of NIH 3T3 fibroblast motility when they were cultured in both adjacent chambers using Model 2 (ii, i.e., fibroblasts vs. fibroblasts). The degree of fibroblast motility was much lower than that of fibroblasts in the heterotypic co-culture model (i, i.e., fibroblasts vs. HepG2 cells in Model 2), but similar to that of fibroblasts in the monoculture Model 1 (iii). All of these results indicate that the effect of increased fibroblast motility was indeed HepG2 induced.

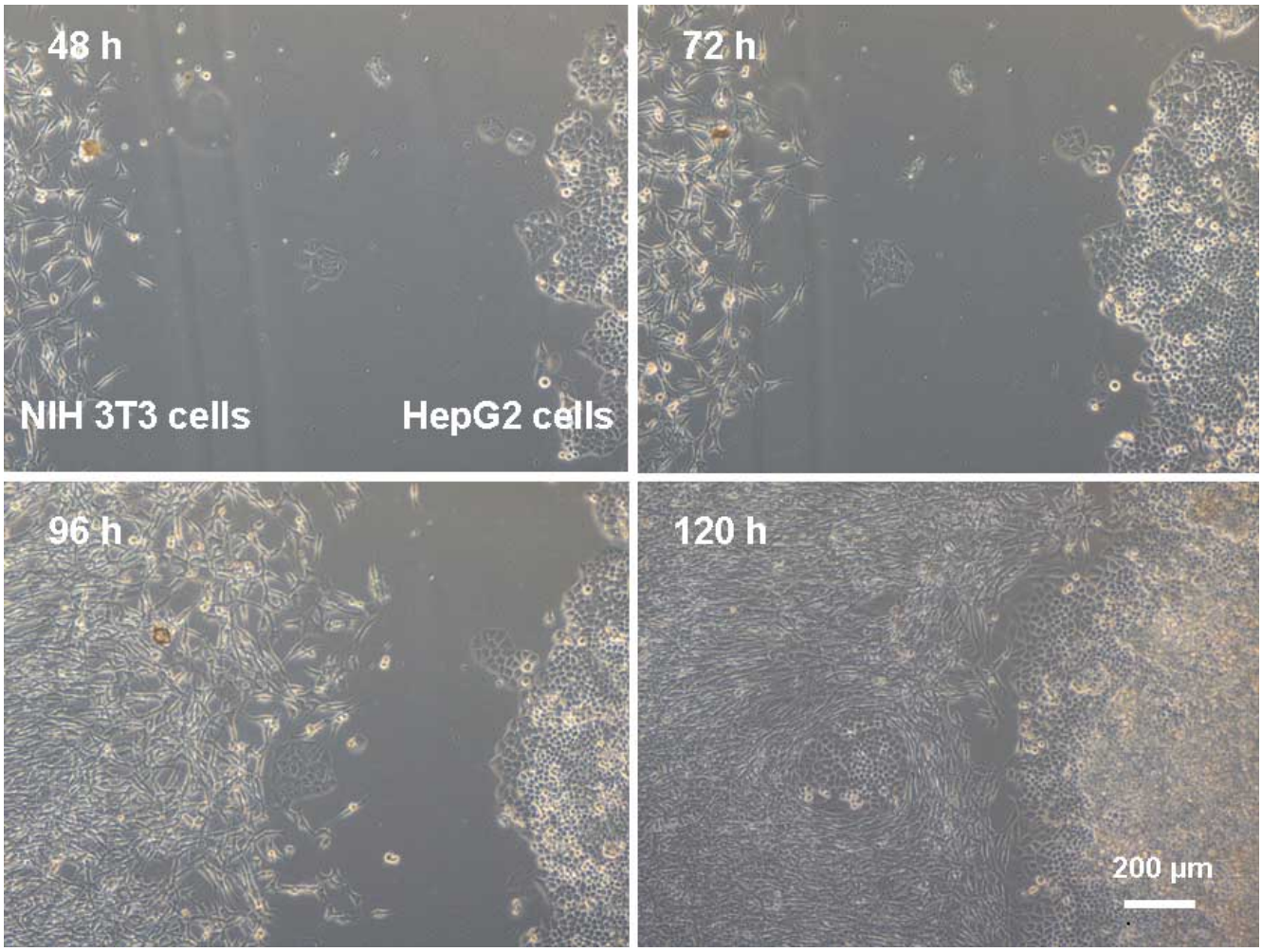

Fig. S8. Cell motility of NIH 3T3 fibroblasts and HepG2 carcinoma cells in an *in vitro* co-culture environment (24-well plate). Two types of cells were positioned artificially using micropipettes. Fibroblasts showed more active migration than HepG2 cells.

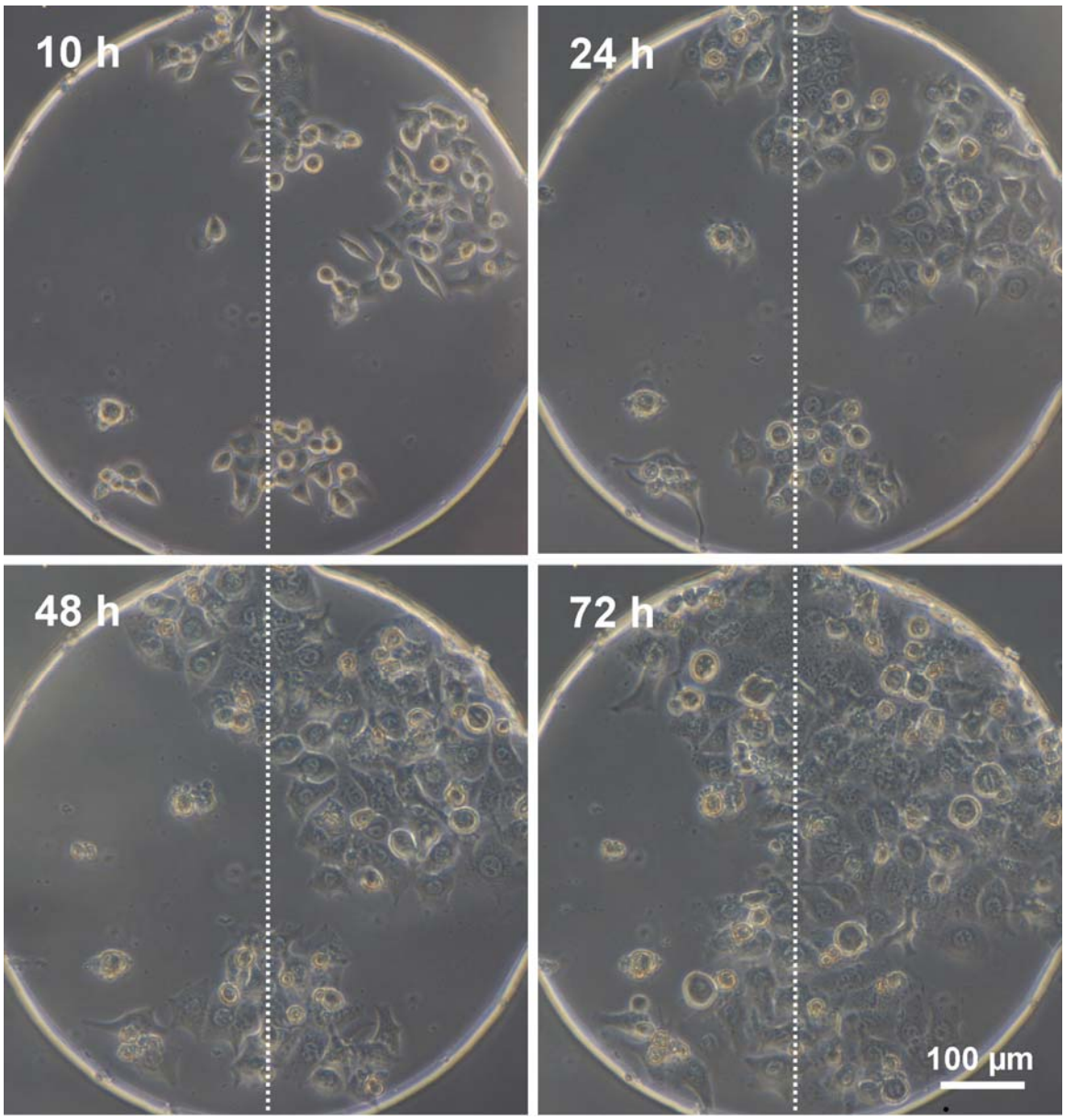

Fig. S9. Culture and proliferation of HepG2 carcinoma cells in the monoculture model (Model 1). It can be seen that HepG2 carcinoma cells adhered and spread within their original region (white lines, right) and then proliferated.

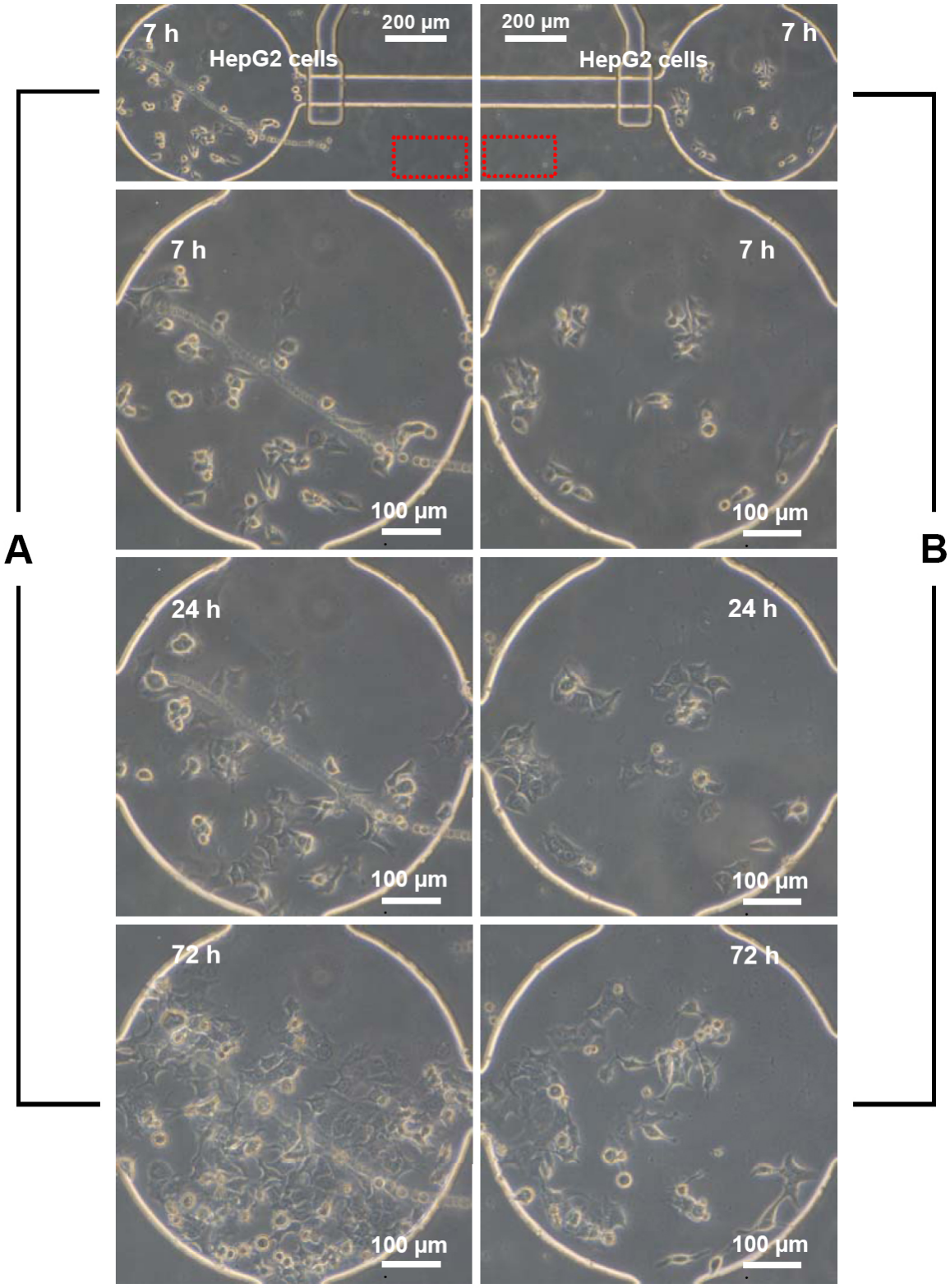

Fig. S10. Culture and proliferation of HepG2 carcinoma cells in both chambers (i.e., HepG2 cells vs. HepG2 cells in Model 2). HepG2 cells in both chambers adhered, spread, and then proliferated normally, which was similar with that shown in Fig. S9 (i.e., HepG2 carcinoma cells in Model 1). The two squares in the red dotted lines in (A) and (B) correspond to the same place in one device.

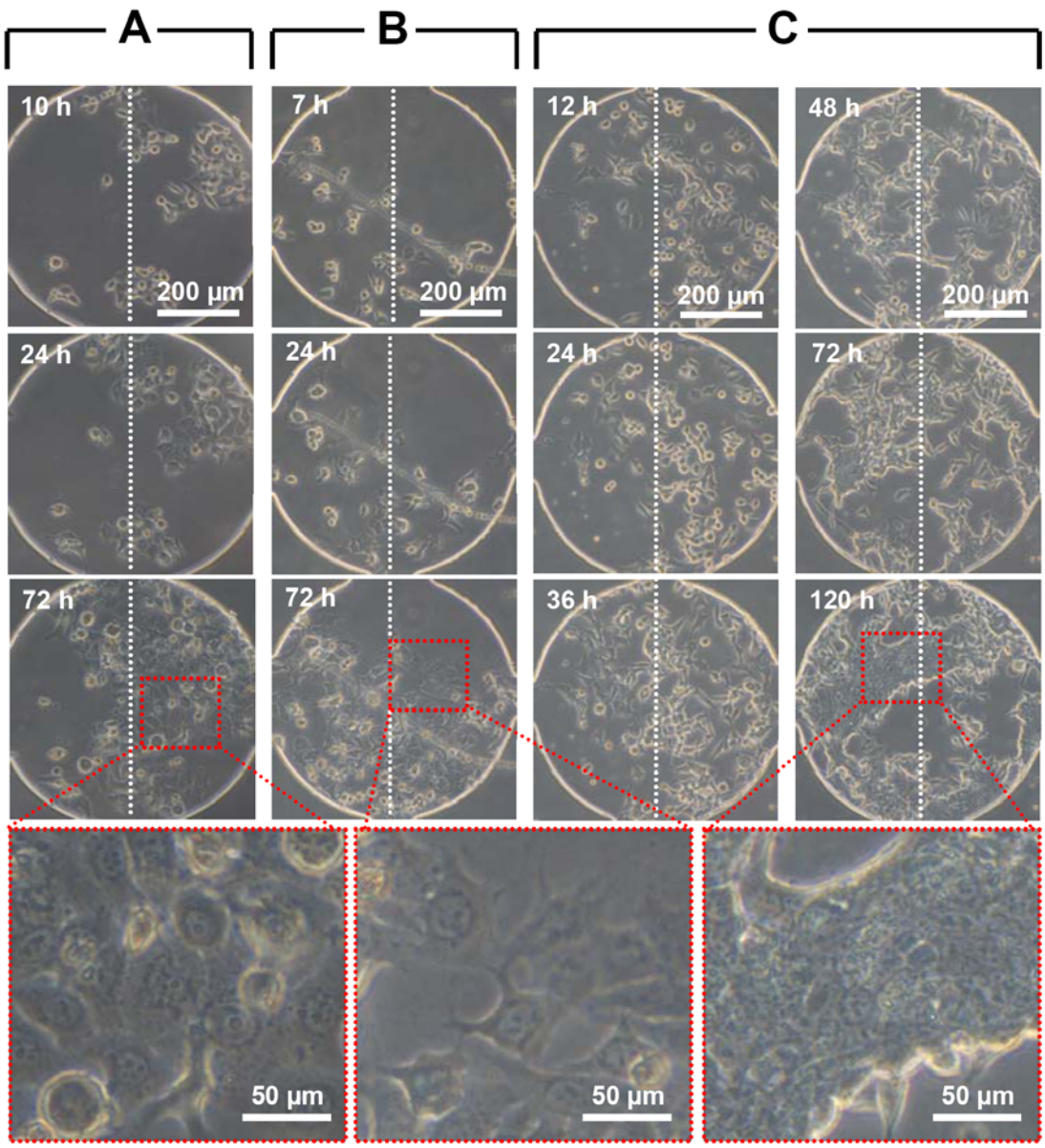

Fig. S11. Comparison of various behaviors of HepG2 carcinoma cells cultured under different conditions. (A) HepG2 cells cultured in Model 1 (corresponding to Fig. S9). (B) HepG2 cells cultured in both adjacent chambers (i.e., HepG2 cells vs. HepG2 cells in Model 2, shown in Fig. S10). (C) HepG2 cells in one chamber cultured using Model 2 with the co-culture of fibroblasts in the adjacent chamber (Fig. 5B in the paper). As can be seen, HepG2 cells adhered and spread normally in both (A) and (B); however, HepG2 cells tended to form spatial aggregations while they were co-cultured with fibroblasts using Model 2 (enlarged images at the bottom of Fig. S11). In other words, the aggregation of HepG2 was the result of 3T3 fibroblast induction.

Analysis of the directional aggregation of HepG2 cells toward 3T3 fibroblasts

To further assay the directional aggregation of HepG2 cells toward the 3T3 cells, the positional variances of HepG2 cells under different conditions (i.e., Model 1, Model 2 with HepG2 cells in both of the adjacent chambers, and Model 2 with HepG2 cells and fibroblasts in the adjacent chambers) were analyzed through cell area analysis. Further, all the images in Fig. S11 were utilized. First, the cell culture chamber was divided into two parts (the left and right halves, Fig. S11, white dotted lines). Then, the areas of HepG2 cells in both halves of the chamber were respectively analyzed using software Image-Pro® Plus 6.0 (Media Cyternetic, Silver Spring, MD), and area changes in HepG2 cells in the two halved places were evaluated using Eqs. (**1**) and (**2**).

$$\text{Percentage of cell area (\%)} = \frac{\text{Total area of cells in a half of one chamber}}{\text{Total area of cells in one chamber}} \times 100 . \qquad \textbf{Eq. 1}$$

$$\text{Variance of cell area (\%)} = \text{Percentage}_{Max} \text{ of cell area (\%)} - \text{Percentage}_{Min} \text{ of cell area (\%)} . \qquad \textbf{Eq. 2}$$

Equation **1** was utilized for cell area distribution analysis in the left and right half areas of one chamber at different experimental times. Equation **2** was utilized for the assessment of the change degree of cell area in the left or right half of one cell culture chamber during the period of each test. Percentage_{Max} and Percentage_{Min} of the cell area respectively represent the maximal and minimal cell area percentage in the left or right half of one chamber during the period of each test. Shown in Fig. S12, the results indicate that NIH 3T3 fibroblasts possessed directional induction to HepG2 aggregation.

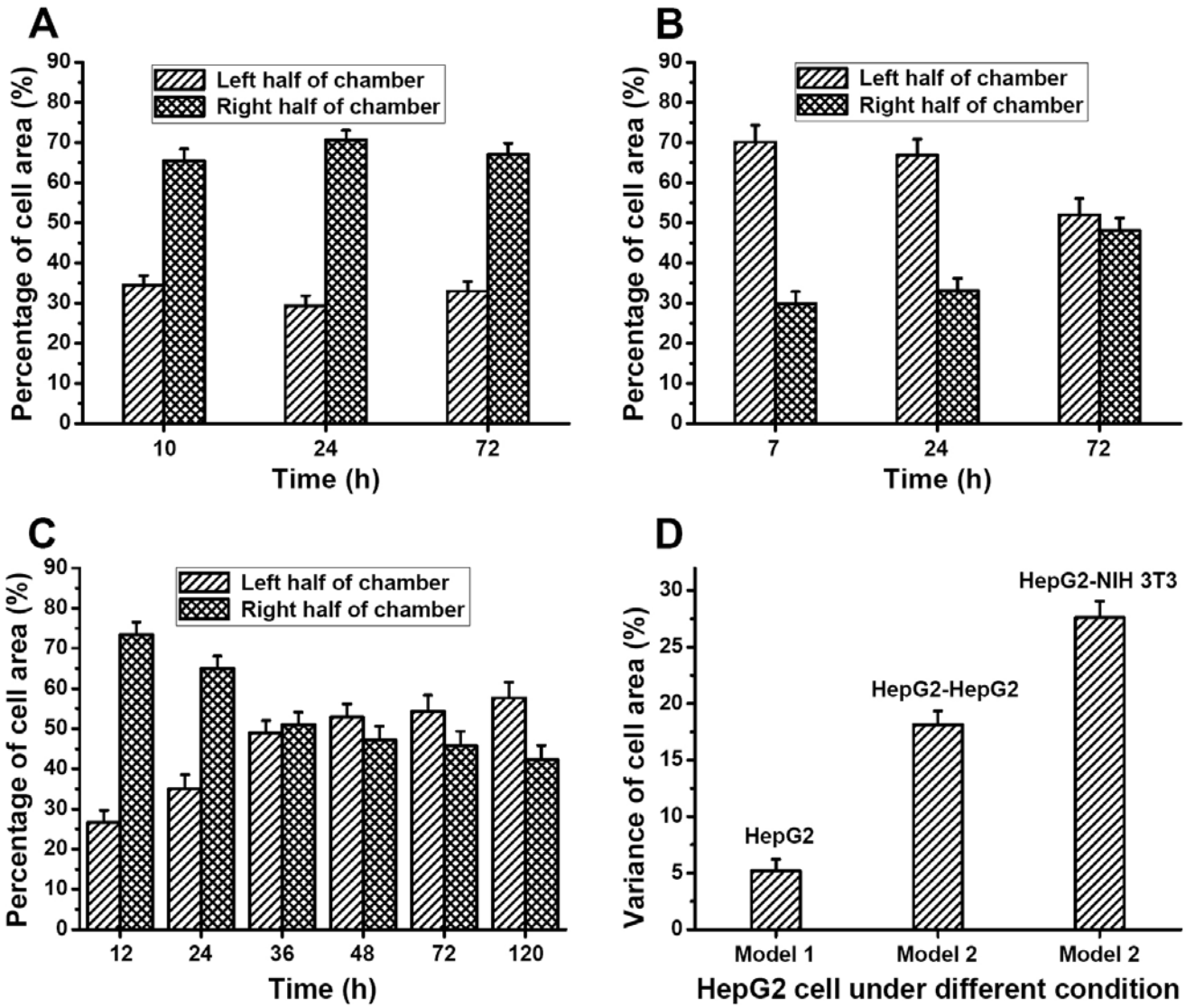

Fig. S12. (A) Percentage of HepG2 cell area in both halves of the culture chamber when HepG2 cells were cultured in monoculture model (Model 1). (B) Percentage of HepG2 cell area in both halves of one chamber when HepG2 cells were co-cultured in both adjacent chambers using Model 2 (i.e., HepG2 cells vs. HepG2 cells). (C) Percentage of HepG2 cell area in both halves of the culture chamber when fibroblasts were cultured in the adjacent chamber using Model 2. (D) Comparison of the variance degree of HepG2 cell area within 72 h in both halves of their culture chamber under the three different conditions mentioned above. Results show that the least area change of HepG2 cells occured in Model 1, and the most change occurred in Model 2 when fibroblasts were co-cultured in the adjacent chamber. Results indicated that NIH 3T3 fibroblasts possessed directional induction to HepG2 aggregation.

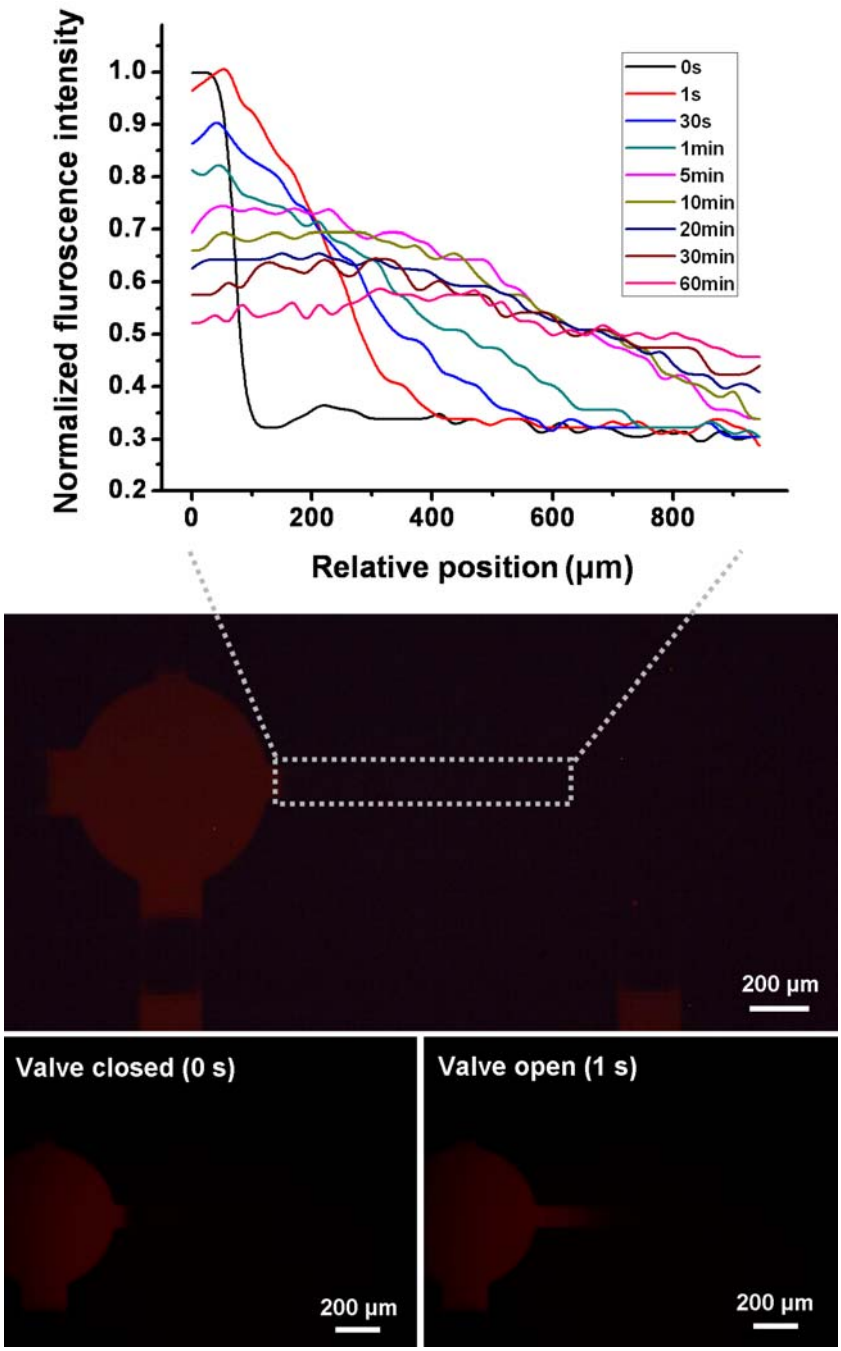

Fig. S13. Regulated chamber communication and visual representation of signal delivery by biomarker (Texas Red-conjugated dextran, 40 kDa, Invitrogen). As can be seen, the biomarker diffused from one chamber to the adjacent one (blank one) through the contact channel while the valves were opened. The first reach took less than 5 min.

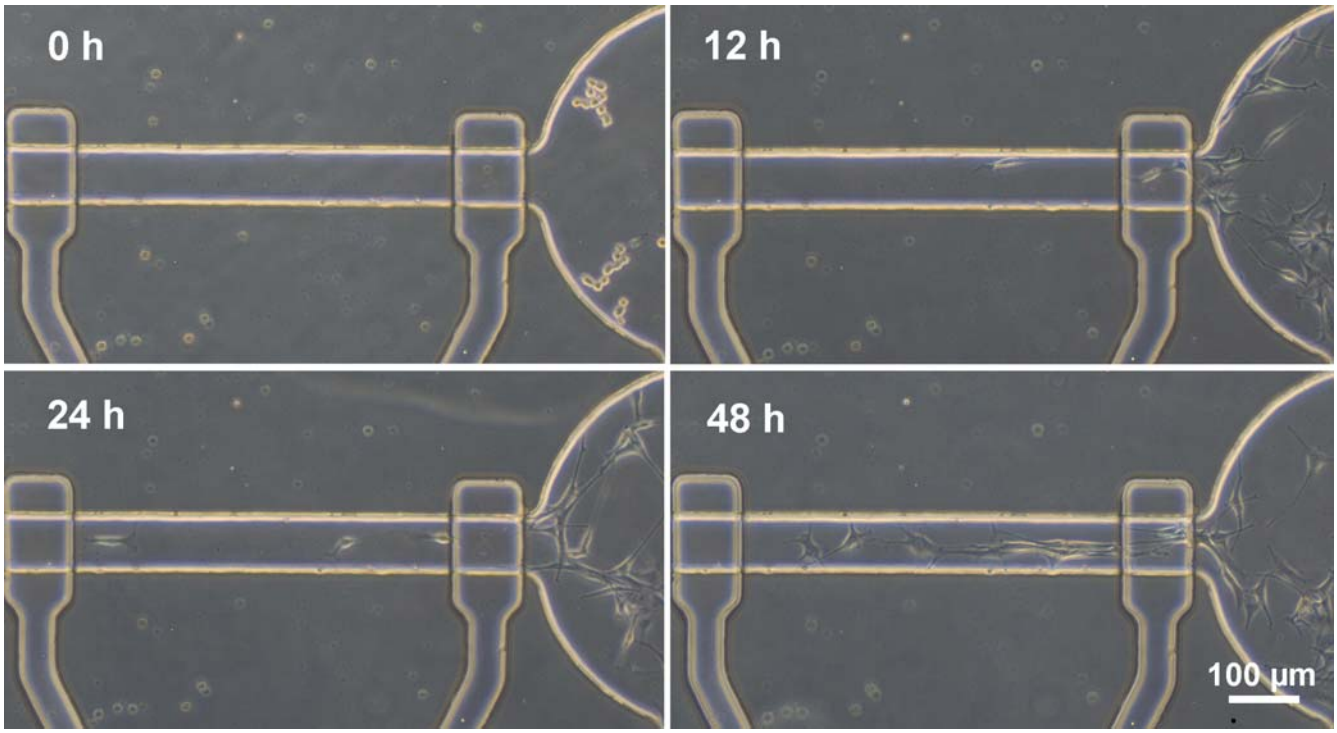

Fig. S14. Directional motility of NIH 3T3 fibroblasts in a cell-soluble condition model (Model 3). We used HepG2 conditioned medium from the 24-well plate as the stimulative which affected the behavior of the fibroblasts. The harvested timing of the conditioned medium was at 72 h, and the initial cell density utilized in the 24-well plate was 5.0×10^4 cells/ml. The fibroblasts clearly showed higher motility compared with those in the co-culture model (Fig. 5 in the paper).

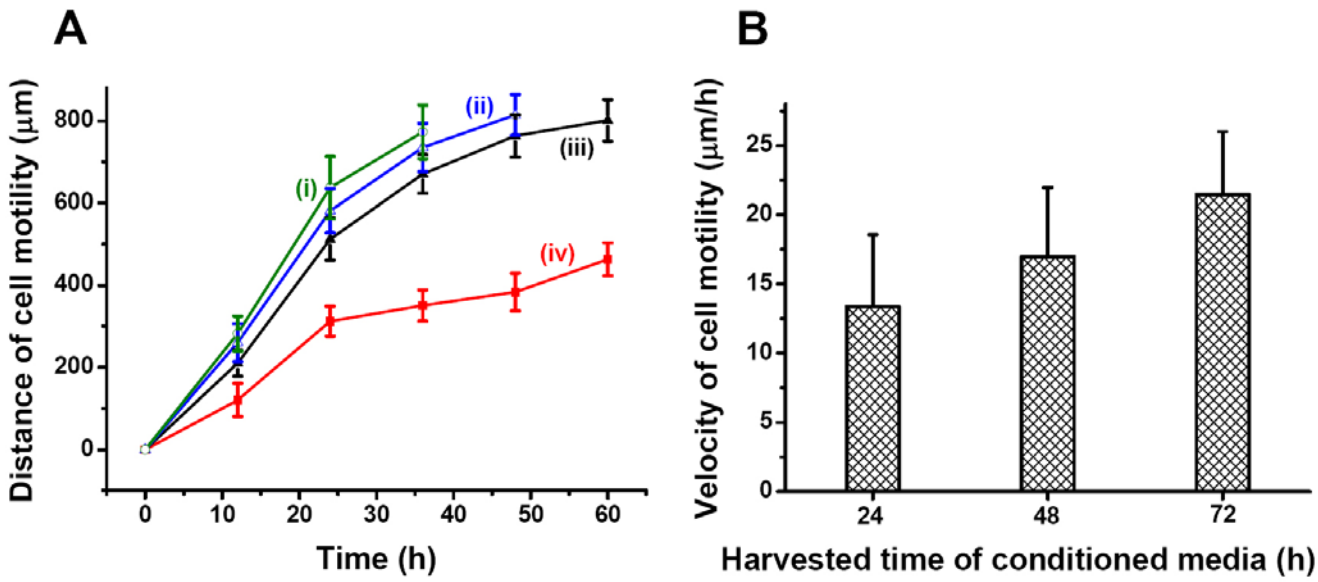

Fig. S15. Assay of NIH 3T3 fibroblast motility under different HepG2 conditioned media harvested from the 24-well plate at different culture times. (A) NIH 3T3 fibroblast motility under HepG2 conditioned media harvested from the 24-well plate at 24 (iii), 48 (ii), and 72 h (i). The initial cell density utilized in the 24-well plate was 5.0×10^4 cells/ml. The data (iv) of NIH 3T3 fibroblast motility in the heterotypic co-culture model (i.e., fibroblasts vs. HepG2 cells in Model 2) were utilized here as controls (Fig. 4A(i) in the paper). As the result shown, the conditioned media caused higher fibroblast migration compared with those in the heterotypic co-culture model (iv). (B) Mean migratory velocity of NIH 3T3 fibroblast under different HepG2 conditioned media harvested from the 24-well plate at 24, 48, and 72 h. The results clearly showed that the harvested time of the conditioned media in the 24-well plate culture environment had a positive correlation to the fibroblast migrating degree. The possible explanation is that higher cell density and more secreted signals of HepG2 cells with longer cultivation induced increasingly higher fibroblast motility.